General Disclaimer

One or more of the Following Statements may affect this Document

- This document has been reproduced from the best copy furnished by the organizational source. It is being released in the interest of making available as much information as possible.

- This document may contain data, which exceeds the sheet parameters. It was furnished in this condition by the organizational source and is the best copy available.

- This document may contain tone-on-tone or color graphs, charts and/or pictures, which have been reproduced in black and white.

- This document is paginated as submitted by the original source.

- Portions of this document are not fully legible due to the historical nature of some of the material. However, it is the best reproduction available from the original submission.

ION-BEAM ANALYSIS OF METEORITIC AND LUNAR SAMPLES[*]

T. A. TOMBRELLO

W. K. Kellogg Radiation Laboratory

California Institute of Technology, Pasadena, California 91125

Abstract

   The unambiguity with which some nuclear reactions may be
identified often permits their use as highly sensitive and selective
analytical tools for the determination of trace element concentra-
tions in complex materials.   In this report examples are given of
the use of charged particle-induced nuclear reactions in attacking
particular problems in astrophysics and planetary science.   These
problems include the determination of elemental abundances of boron
and fluorine in carbonaceous chondritic meteorites, the identifica-
tion of products of lunar vulcanism, and the study of solar wind-
implanted atoms in lunar materials.   This technique will be seen to
be an important supplement to other methods of elemental and isotopic
analysis — especially for cases involving light elements at very low
concentrations and where high resolution depth distribution informa-
tion is needed in non-destructive analyses.
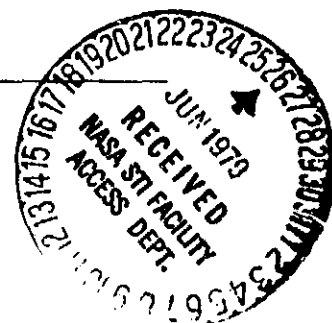
1. Introduction

It seems particularly appropriate that this paper be presented now, because it is almost exactly ten years ago that we began to employ nuclear reactions in the analysis of extraterrestrial materials. It is, of course, no accident that our initiation of these researches coincided with the successful return of samples from the moon by the Apollo 11 mission. In this paper I shall review our slow progress during this decade to solve a few planetary problems for which these techniques proved to be especially applicable. These examples have been selected because they show how ion-beam analysis can be used by itself as an analytical technique on the original samples. However, one is not limited to just such cases, and usually a combination of several analytical methods will be required for the solution of the problem at hand.

Much of the material reviewed here has previously been published; however, since it has appeared in the journals of a number of scientific fields, this summary may provide a useful introduction for anyone who wishes to apply our ideas elsewhere.

2. Meteorites

For those who are interested in stellar phenomena, the abundances of the chemical elements and their isotopes provide many clues about the environments in which they were created. Knowledge of relative universal abundances of the elements comes mainly from two sources: spectroscopic analyses of the atomic transition lines from stars and chemical analyses of samples from carbonaceous chondritic meteorites. For the most part, terrestrial samples have been so fractionated chemically by aeons of geological processing that

1

they are of limited value in determining universal abundances. The carbonaceous chondrites are thought to be condensates from the evolving solar nebula that have undergone little subsequent modification; thus, they are expected to be an accurate representation of the abundances of the non-volatile elements at the time of solar system formation. These meteorites resemble the solid material expected when a gas cloud of solar composition cools to temperatures of ~ 300 °K at low pressures (10^{-4} to 10^{-6} atmospheres)[1]). Elements that are gases at these temperatures (C, N, O, noble gases, and perhaps chlorine) are depleted in these meteorites relative to the sun, whereas there is usually good agreement between solar photospheric abundances of nongaseous elements and the corresponding meteoritic abundances[2,3]). Cases in which particular elements are enriched in meteorites provide important clues about solar structure. For example, the 200-fold enrichment of Li is generally regarded as indicating thermonuclear destruction of solar Li, either in an early convective period of solar evolution or by burning at the base of the surface convection zone during the main sequence lifetime of the sun[4,5]).

2.1. BORON IN CARBONACEOUS CHONDRITES

There are three elements that lie far below the abundance curve established by the other elements — Li, Be, and B. Because these elements have low Coulomb barriers and very large (p,α) cross sections, they are easily destroyed in the central regions of stars. Thus, we think that these elements must have been created in non-stellar astrophysical processes: ^{7}Li was produced mainly in the Big Bang; and the others (^{6}Li, ^{9}Be, and ^{10,11}B) were made by proton and alpha-particle spallation reactions from cosmic rays striking material in the interstellar medium.

The abundances of Li and Be are reasonably well known, but B analyses

were considered suspect because of the large disagreement between the solar
and meteoritic abundances. (The abundances of Be obtained from these two
sources agree, making it unlikely that B is burned in the sun if Be is not.)
Measurements of boron in the solar photosphere[6,7], the interstellar medium[8],
and Vega[9] give values of $B/H \sim 10^{-10}$, while Cameron et al.[10] have calcu-
lated a meteoritic value of $B/H = 1.5 \times 10^{-8}$ based on the carbonaceous
chondrite analyses by Quijano-Rico and Wänke[11]. As emphasized by Cameron
et al.[10], a B/H value of 10^{-8} is much too high to be compatible with the
otherwise attractive theories of galactic cosmic-ray nucleosynthesis of Li,
Be, and B[12,13]. Thus, it became desirable for us to check the B meteoritic
abundance with a different experimental technique.

Our ^{11}B analyses serve as an example of how a well-known nuclear reaction
can be used in a new context. The $^{11}B(d,p)^{12}B$ reaction was an obvious choice
since it has a large cross section (~ 0.5 barn) and an easily distinguished
final product, ^{12}B (20 msec half life, 13 MeV beta end point energy)[14].
Nevertheless, the fact that the B must be detected in the presence of a
million times more other material in the sample keeps it from being a trivial
exercise. The detection apparatus is quite simple: a plastic scintillator,
its associated electronics, and some single channel analyzers and scalers.
Figure 1 shows the bombardment and counting sequence, as well as an example
of the raw and subtracted data[15]. The meteoritic sample is irradiated in
pulses 30 msec long with 2.8 MeV deuterons from the ONR-CIT tandem accelerator.
During the 75-msec period between pulses, there is a short delay after which
there are four 15-msec counting periods for the plastic scintillator, which
is located directly behind the activated sample. In order to discriminate
against lower energy betas and gamma rays from other activities, only counts
above 6 MeV are analyzed. The ^{11}B concentration can be calculated from the

counts in the four counting periods, after correcting for the decay of the background (due mainly to ^{16}N and ^8Li). We have a signal to noise of only ~ 1/20 for 1 ppm (wt) boron — most of the background coming from the highest energy branch of the ^{16}N produced in the reaction $^{18}O(d, \alpha)^{16}N$. This reaction has a small cross section, but since meteoritic material is about 50% oxygen, the ^{16}N contribution becomes serious. Fortunately, the ^{16}N lifetime (7.2 sec) is so different from that of ^{12}B that we can separate the two decay contributions, but a large number of counting cycles (~ 5×10^4) are required to give a 15% standard deviation on samples containing 1 ppm boron. Absolute concentrations were obtained using reference samples of the National Bureau of Standards glass SRM 610, for which B has been determined by isotopic dilution.

It was important to establish that the data were not seriously affected by contamination. We knew that a source of contamination was present because when we re-analyzed a given sample (meteorite or control) after prolonged exposure to the atmosphere, the measured boron concentration had increased, sometimes by as much as a factor of 2-3. Even precautions in the storage of the samples between irradiations often failed to prevent this increase. Consequently, all reported results are based on the first analyses of freshly prepared samples. The source of the contamination is not certain; however, it is clearly airborne and limits on the size of the contaminating particles have been set using nuclear track counting for the reaction $^{10}B(n, \alpha)^7Li$ (ref. [16]). These data indicated an upper limit of $\leq 10^9$ atoms of boron per contaminant particle. The most likely form of such small contaminant particles is aerosol droplets, e.g., sub-micron H_3BO_3 solutions, presumably originating from sea spray. An observed correlation between high boron results for control (as well as meteorite) samples and certain local weather patterns suggests a second possible source of contamination. Extensive

borate deposits are located in the nearby deserts, and it is likely that fine
dust particles from these deposits are blown into our area by the occasional
strong winds from that direction.

A number of tests performed indicated that negligible boron contamination
was acquired during the normal exposure and storage of freshly prepared
samples prior to analysis. They also show that meteorite samples did not
acquire boron contamination more rapidly than the control samples. However,
these results did not preclude the possibility that "instantaneous" contamina-
tion occurred when the meteorite surface was first exposed to the atmosphere.
To investigate this possibility, several slices from the Murchison meteorite
were analyzed. Following the initial analyses, fresh surfaces were scraped
on the samples without breaking the vacuum, and the samples were then re-
analyzed. This procedure was repeated several times, yielding the results
shown in fig. 2. Although one sample (#3) was seriously contaminated
initially, the boron concentrations found after several scrapings were well
within the normal range of concentrations found for this meteorite. Our
results for six meteorites are shown in fig. 3.

The final column in table 1 gives gives the relative atomic B/H ratio
calculated in the standard way, using Si as an intermediate normalization:
$(B/H) = (B/Si)_{met} (Si/H)_{sun}$, where we have used Si contents for individual
meteorites or average Si contents for the various meteorite subgroups. The
value of $(Si/H)_{sun} = 4.5 \times 10^{-5}$ that we used was taken from ref. 3. Our
results clearly indicate a B/H ratio of $2 \pm 1 \times 10^{-9}$, which is in disagreement
with the values of 10^{-8} proposed in ref. 10 and the 10^{-10} upper limit for the
solar photosphere obtained in ref. 6. (The uncertainty indicated for our re-
sult arises because of the variation in B/Si for the various meteorites; the
precision for an individual meteorite is much better.) Our result is, however,
in reasonable agreement with the recent solar value of Kohl et al. or
$4^{+4}_{-2} \times 10^{-10}$ (ref. [7]). (It is worthy of note that the high B concentrations

5

obtained in ref. 11 may have been due to the location of the laboratory in the neighborhood of a glass factory that produces high boron glass[17]).)

2.2. FLUORINE IN CARBONACEOUS CHONDRITES

As discussed in the preceding section, carbonaceous chondritic meteorites are believed to closely resemble the average solar system element concentration. Previous work has given a large range of fluorine concentrations in meteorites[18-20] and all values were high when compared to solar or cosmic ray abundance data (see, for example, Teegarden et al.[21]).

Thus, it was important to repeat the fluorine analyses with a different technique; in this case, the $^{19}F(p,\alpha\gamma)^{16}O$ reaction at the resonance at E_p = 872 keV was a logical choice because of its large cross section and adequate depth resolution[22]. The high yield made it possible to detect fluorine unambiguously at low concentrations; knowledge of the distribution of fluorine versus depth allowed any surface contamination present to be separated from the bulk fluorine concentration. With reasonable care, we were able to eliminate contamination in the sample preparation and handling, and all samples showed a flat distribution of fluorine with depth and no surface peaks[23].

One must remember that meteorites are not homogeneous in their structure or composition; thus, care must be taken to insure that local differences in concentration are averaged out. Two types of sample were used: chipped or sawed solid slices; and crushed and homogenized ($<$ 75 μm grain size) samples that were pressed into pellets. The results of these measurements are given in table 2. The interconsistency of the Murchison solid slices is clearly demonstrated. From the homogenized samples we obtain for $F/10^6$ Si atoms the values: C1, 1009; C2, 755; and C3, 559. These results indicate a lower solar system abundance for fluorine than found previously[18-20],

6

and the value we obtain is in good agreement with the solar photospheric
F abundance.

3. Surface Studies of Lunar Materials

Since 1969 our group has also exploited the use of nuclear techniques
to investigate a series of problems arising in the analysis of returned lunar
samples. The overall goal of this research is to understand and to sort out
the relative importance of the various mechanisms which influence the chemical
and physical properties of the outer few microns of the lunar surface, viz.,
solar particle implantation and subsequent redistribution, sputtering and
micrometeorite erosion, and deposition from the lunar atmosphere either as
atomic vapors or as low energy ions formed by ionization of atmospheric
constituents by solar electrons or photons.

The outer micron represents a negligible portion of the mass of the moon.
The justification for research on such an insignificant fraction is that the
outer micron is the interface between the moon and the rest of the solar
system. Unique processes, such as solar wind implantation and erosion, have
affected this layer and have produced unique materials as far as terrestrial
experience is concerned. The lure that has drawn many of us into the analysis
of lunar samples is that the record of over three billion years of solar and
solar system history is held in them. We have the hope that with sufficient
cleverness we can decipher that recording.

3.1. SOLAR WIND HYDROGEN IN LUNAR SAMPLES

By using the resonant nuclear reaction $^1H(^{19}F, \alpha\gamma)^{16}O$ (at the $E_p =$
872 keV resonance) we have been able to measure the depth profile for hydrogen

in the surfaces of lunar samples[25,26]). Figure 4 shows a typical result for
a surface chip from an Apollo 16 rock[26]). Although implantation of solar
wind hydrogen is the most likely original source, the observed profile ex-
tends to a significantly greater depth than would be expected from the direct
implantation of 1 keV solar wind protons. This is in agreement with con-
clusions based on chemical etching experiments for implanted noble gases[27-29]).
If solar wind is the source of this hydrogen component, extensive modifica-
tion by diffusion and trapping of hydrogen atoms is implied. If diffusion
rates for hydrogen in terrestrial silicates[30]) are applicable to the lunar
samples, it appears that bulk volume diffusion would be too rapid to result
in the observed profiles without some sort of trapping to slow down the
diffusion process[31]). A model in which solar wind hydrogen diffuses rapidly
into (and out of) the samples with a small remnant of the implanted dose being
retained in radiation damage traps seems plausible. The radiation damage is
evidently so heavy in the outer 500 Å that few isolated traps remain[32]). At
greater depths intense radiation damage (but below saturation) may persist
to a depth of $\sim$ 2000 Å, corresponding closely with the radiation damage range
of He ions with velocities near those of frequent high velocity (up to
800 km/sec) solar wind streams observed in satellite experiments[33]). The
population of isolated radiation damage traps by diffusing solar wind atoms
may thus result in a depth profile that reflects the distribution of radia-
tion damage. A discontinuity in the radiation damage gradient near 2000 Å
may account for the characteristic bend observed in the measured hydrogen
profiles, with the tail of the hydrogen distribution below 2000 Å representing
diffusion into a region in which the radiation damage (due to solar flare
and suprathermal ions) is much less intense.

In practice it has proved impossible to extract any detailed information about solar wind processes from the hydrogen profiles observed; however, there is an excellent correlation between the observation of a profile like that in fig. 4 and a long lunar surface exposure of that face of the sample. Conversely, samples that show little implanted (or trapped) hydrogen also have short exposure ages (as confirmed, for example, by the density of micro-meteorite pits in their surfaces).

3.2. FLUORINE LAYERS ON LUNAR SAMPLES

The success of the meteorite work convinced us that we could apply the F analysis to other planetary problems. The most obvious application involved a controversy about the moon's history; in addition to the obvious effects of meteorite impact, was there any clear-cut evidence of lunar vulcanism? ^{19}F is virtually non-existent in the solar wind, and the bulk concentration of ^{19}F in lunar rocks is quite low (a few hundred ppm). Since halogens are frequently a component of terrestrial volcanic gases, the presence of fluorine surface films on lunar samples might represent an indication of the surface deposition of volcanic vapor.

Using the ^{19}F$(p,\alpha\gamma)^{16}$O reaction at the $E_p = 872$ keV resonance we have found F surface deposits on Apollo 15 green glass, Apollo 17 orange glass, and on vesicle (bubble) linings from Apollo 15 basalts. Surface layers of about 10^{15} F atoms/cm^2 were seen on unbroken spheroidal (~ 0.1 mm diameter) surfaces of the green and orange glasses, whereas thinner ($\sim 10^{14}$ F atoms/cm^2) deposits were found on vesicle linings[34]). Figures 5 and 6 show examples taken from runs on green glass spheres as well as on the lining from a vesicle from an Apollo 15 rock. It can be conclusively shown that the F deposits are lunar and not due to fluorocarbon contamination[35]), because brown glass fragments

from the same collected sample do not show a F surface peak, and when the beam is off the vesicle surface the rock does not show a surface F peak.

The presence of vesicles and vugs (bubbles that break through the surface) in lunar rocks demonstrates the existence of lunar magmatic vapors. In fact, some of the mare basalts (e.g., 15018 and 15556) are about 50% vesicles. It is also quite likely that the Apollo 15 green and Apollo 17 orange glasses were produced by the eruption of such gas-rich lunar magmas[36]. Nothing similar to the green or orange glass occurs on the earth, probably because the absence of water and an atmosphere makes a lunar vulcanism different from on earth. One conjecture about the mechanism is a lava fountain that sprayed molten glass and vapor into the vacuum; as the small glass spheres solidified and fell back through the vapor cloud they were coated with the observed volatile chloride, fluoride and sulfide layers[36]. Exposure to hot water does not remove the F deposits on the green or orange glasses, which rules out many simple fluoride salts as the chemical form for the surface films. Direct F fixation in the glass is possible, either by the action of lunar HF vapor or by hydrolysis of a reactive fluoride layer upon exposure to the terrestrial atmosphere[34]. These small green and orange glass balls are probably the most unusual material that was returned from the moon, and we shall be involved in attempts to understand its specific origin for a long time.

3.3. SOURCES OF LUNAR CARBON

In our concern with lunar vulcanism and the magmas that resulted from the large impact craters, it was important to identify the gases that produced the vesiculation in lunar rocks. By the process of elimination, we became convinced that the major contribution came from carbon monoxide (CO)[34], which led to the problem of understanding the abundance of lunar carbon. The basic

difficulty is that we do not understand why there is so little carbon on the moon; there are three sources (the solar wind, impact of carbonaceous chondritic meteorites, and indigenous), each of which could easily have supplied as much carbon as is there now. Thus, we needed to investigate the various sources and loss mechanisms for lunar carbon.

We required a technique that not only has high sensitivity but which also has sufficient depth resolution to separate surface carbon (implanted solar wind or volcanic vapor deposits) from carbon in the bulk (indigenous or re-distributed surface carbon). After several false starts, we found that the $^{12}C(d,p)^{13}C$ reaction offered the best overall characteristics[37]).

Figure 7 gives a schematic description of the technique[38]). The proton spectrum is observed; protons that originate near the surface have higher energies than those from greater depths due to the energy loss of the incident deuterons and the protons. With this technique surface carbon layers of about 10^{13} atoms/cm^2 and volume concentrations of less than 10 ppm (wt) can be observed; the depth resolution is ~ 1000 Å (ref. [38])).

A serious contamination problem arose immediately; even interior samples from lunar rocks exhibited surface carbon layers of $\sim 10^{15}$ atoms/cm^2. This was eventually traced to the adsorption of CO or CO_2 on the sample surfaces. This occurred even for samples that had been handled exclusively in clean N_2 and transferred without atmospheric exposure into our vacuum system ($\sim 10^{-10}$ torr). After several failures, we found that the adsorbed CO or CO_2 could be removed without disturbing the implanted carbon under low intensity bombardment with a 2 MeV ^{19}F ion beam. Figure 8 shows the result of a control test for a radiation damaged quartz sample. This "sputter" cleaning process works well for both silicate and metallic surfaces; it is very likely that it involves enhanced desorption rather than sputtering, but we do not yet understand the mechanism in detail. The removal of carbon

11

proceeds at a rate that is several orders of magnitude greater than that of ordinary sputtering.

Recently we have applied the cleaning and analysis techniques in the study of lunar breccias[38]), which are materials formed from fine soil particles welded together by molten glass from meteoritic impacts. Figure 9 shows a typical proton spectrum from a breccia sample with the contributions from the carbon and other elements that affect the line shape. Because the samples are quite rough at the microscopic level, the spectrum shape is somewhat different from that of a smooth target. Figure 10 shows a typical decomposition of a spectrum (using the standard line shapes from control samples) into "surface" and volume components.

Some of the systematic features of the samples are beginning to appear; fig. 11 shows the surface concentration versus volume concentration for a number of lunar breccias. The surface exposure (probably from implanted solar wind carbon) is relatively constant, but the volume component is highly variable. What this probably means is that solar wind (and perhaps meteoritic carbon) are gradually converted into volume carbon as the soil matures, the approximately constant surface density representing an equilibrium that is quickly established ($\sim 10^4$ years). Thus, we have made a start on the problem, but now must find a way to separate the surface contributions from meteorites and solar wind. In addition, it would be helpful to find a way to estimate the fraction of carbon that is retained on the lunar surface after a meteorite impact.

4. Conclusions

For the examples presented here, two characteristics of nuclear reactions have proved to be especially important. The first is selectivity, the ability to observe a given reaction even though the target nucleus is only a minor constituent in a complex material. This selectivity may arise because of a large nuclear reaction cross section and/or an easily identified final product. This selectivity is essential because you have virtually no control over the composition of the sample being analyzed; one must take what Nature provides.

The second characteristic is the depth dependence of some nuclear reactions. This ability to separate contributions to the yield from the sample surface and the interior permits the identification of contaminants that have been introduced in either collection or handling. The depth profile has also been shown to provide information that is necessary for the separation of contributions from different geological processes, each of which may affect the surface and bulk concentrations in different ways.

5. Acknowledgments

13

References

1) L. Grossman and J. W. Larimer, Rev. Geophys. Space Phys. 12 (1974) 71.

2) E. Anders, Ann. Rev. Astron. Astrophys. 9 (1971) 1.

3) J. E. Ross and L. H. Aller, Science 191 (1976) 1223.

4) W. Nichiporuk, in Elemental Abundances in Meteorites ed. B. Mason; Gordon and Breach, New York, 1971) p. 67.

5) N. Grevesse, Solar Phys. 5 (1968) 159.

6) D. N. B. Hall and O. Engvöld, Astrophys. J. 197 (1975) 513.

7) J. L. Kohl, W. H. Parkinson and G. L. Withbroe, Astrophys. J. Letters 212 (1977) 101.

8) D. C. Morton, A. M. Smith and J. P. Stecher, Astrophys. J. Letters 189 (1974) 109.

9) A. M. Boesgaard, F. Praderie, D. S. Leckrone, R. Faraggiana and M. Hack, Astrophys. J. Letters 194 (1974) 143.

10) A. G. W. Cameron, S. A. Colgate and L. Grossman, Nature 243 (1973) 204.

11) M. Quijano-Rico and H. Wänke, in Meteorite Research (ed. P. M. Millman; Reiden, Dordrecht, 1969) p. 132.

12) H. Reeves, W. A. Fowler and F. Hoyle, Nature 226 (1970) 727.

13) M. Meneguzzi, J. Audouze and H. Reeves, Astron. Astrophys. 15 (1971) 337.

14) R. W. Kavanagh and C. A. Barnes, Phys. Rev. 112 (1958) 503.

15) M. R. Weller, M. J. Furst, T. A. Tombrello and D. S. Burnett, Geochim. Cosmochim. Acta 42 (1978) 999.

16) M. R. Weller, M. J. Furst, T. A. Tombrello and D. S. Burnett, Astrophys. J. Letters 214 (1977) 39.

17) H. Wänke, private communication.

18) D. E. Fisher, J. Geophys. Res. 68 (1963) 6331.

14

19) G. W. Reed, Geochim. Cosmochim. Acta $\underset{\sim}{28}$ (1967) 1239.

20) L. Greenland and J. F. Lovering, Geochim. Cosmochim. Acta $\underset{\sim}{29}$ (1965) 821.

21) B. J. Teegarden, T. T. von Rosenvinge and F. B. McDonald, Astrophys. J. $\underset{\sim}{180}$ (1973) 571.

22) D. A. Leich, T. A. Tombrello and D. S. Burnett, Proc. Lunar Sci. Conf. 4th, Vol. 2 (1973) p. 1597.

23) R. H. Goldberg, D. S. Burnett, T. A. Tombrello and M. J. Furst, Meteoritics $\underset{\sim}{9}$ (1974) 347.

24) D. N. B. Hall and R. W. Noyes, Astrophys. Letters $\underset{\sim}{2}$ (1969) 235.

25) D. A. Leich and T. A. Tombrello, Nucl. Instr. and Meth. $\underset{\sim}{108}$ (1973) 67.

26) D. A. Leich, R. H. Goldberg, D. S. Burnett and T. A. Tombrello, Proc. Lunar Sci. Conf. 5th, Vol. 2 (1974) p. 1869.

27) P. Eberhardt, J. Geiss, H. Graf, N. Grögler, U. Krähenbuhl, H. Schwaller, J. Schwarzmuller and A. Stettler, Proc. Apollo 11 Lunar Sci. Conf. (1970) p. 1037.

28) T. Kirsten, O. Müller, F. Steinbrunn and J. Zähringer, Proc. Apollo 11 Sci. Conf. (1970) p. 1331.

29) H. Hintenberger, H. W. Weber, H. Voshage, H. Wänke, F. Begemann and F. Wlotzka, Proc. Apollo 11 Lunar Sci. Conf. (1970) p. 1269.

30) R. Brückner, J. Non-Crystalline Solids $\underset{\sim}{5}$ (1971) 117.

31) H. Ducati, S. Kalbitzer, J. Kiko, T. Kirsten and H. W. Müller, The Moon $\underset{\sim}{8}$ (1973) 210.

32) J. Borg, M. Maurette, L. Durrieu and C. Jouret, Proc. Lunar Sci. Conf. 2nd (1971) p. 2027.

33) J. H. Wolfe, Solar Wind, NASA SP-308 (1972) p. 170.

34) R. H. Goldberg, T. A. Tombrello and D. S. Burnett, Proc. Lunar Sci. Conf. 7th (1976) p. 1597.

35) R. H. Goldberg, D. S. Burnett and T. A. Tombrello, <u>Proc. Lunar Sci. Conf. 6th</u>, Vol. 2 (1975) p. 2189.

36) D. S. McKay, U. S. Clanton and G. H. Ladle, <u>Proc. Lunar Sci. Conf.</u> 4th (1973) p. 225.

37) R. H. Goldberg, Ph.D. thesis, California Institute of Technology (1976) unpublished.

38) C. Filleux, T. A. Tombrello and D. S. Burnett, <u>Proc. Lunar Sci. Conf. 8th</u>, Vol. 3 (1977) p. 3755.

39) C. Filleux, R. H. Spear, T. A. Tombrello and D. S. Burnett, <u>Proc. Lunar Sci. Conf. 9th</u>, Vol. 2 (1978) p. 1599.

TABLE 1

Average B concentrations in carbonaceous chondrites

Meteorite	Type	Samples Analyzed	Average B (ppm, wt)	Atomic B/Si (10^{-6})
Ivuna	C1	1	3.0	77
Orgueil		1	1.6	40
Murray	C2	6	1.4	29
Murchison		12	1.7	35
Allendé	C3-4	9	1.8	23
Lance		2	1.5	19

TABLE 2

Fluorine concentration data for carbonaceous chondrite meteorites. Since no samples exhibited surface peaks, concentrations quoted are taken from net average yields over the resonance. Typical analytic precision is ± 8%. Carbonaceous chondrite type is also indicated.

Solid Samples

Sample	ppmF	F concentration atoms F/10^6 atoms Si
Murchison*	80	910
Murchison 7b*	72	819
Murchison 7c*	73	830
Murchison 7d*	80	910
Murchison 7e*	53	603
Murchison 7f*	93	1058
Allendé 21-14[†]	165	1562
Allendé 21-15[†]	94	890
Murchison average	75.2	855
Allendé average	129.5	1226

Crushed Samples

Sample	ppmF	F concentration atoms F/10^6 atoms Si
Murchison 5*	75	853
Murchison 6*	60	682
Murchison 10*	66	751
Murchison 11*	59	671
Mighei*	66	751
Essebi*	80	910
Haripura*	59	671
Ivuna‡	70	981
Orgueil‡	74	1037
Allendé[†]	59	559
Murchison average	65	739
Type II average	67	762
Type I average	72	1009
All crushed average	67	787

‡ carbonaceous chondrite Type I; * carbonaceous chondrite Type II; [†] carbonaceous chondrite Type III.

18

Figure Captions

Fig. 1. a) The counting cycle for the ^{12}B pulsed beam activation measurement. The delays between 0-7 and 30-45 msec are to insure that the beam is totally deflected. The Y values indicate the number of counts in the four successive counting intervals after beam deflection. The decrease from Y_1 to Y_4 schematically indicates the ^{12}B decay.

b) An example of an uncorrected decay curve for a meteorite (Ivuna) sample. Decay time is measured after the start of interval Y_1 (fig. 1a).

c) A background corrected decay curve of the data from fig. 1b. The corrected activity follows the 20 msec decay of ^{12}B.

Fig. 2. This figure shows the results of vacuum-scraping tests on three samples from the Murchison meteorite. The data from Sample #1 indicate no contamination. Although Sample #3 showed considerable surface contamination initially (the boron concentration before scraping was 7 ppm), the relatively constant ultimate values are within the range of concentrations found for other samples of this meteorite. The concentrations shown for Sample #2 are 10-20% below the actual values, because these runs had a slightly higher threshold on the beta detector.

Fig. 3. Measured boron concentration in different pieces of six carbonaceous chondrites. X's indicate measurements of homogenized aliquots of a single specimen. Errors for these samples are approximately the same as the errors for other samples having an equivalent B concentration. Reproducibility between aliquots

is good. The relatively small spread between different specimens of the same meteorite indicates that our results are not significantly influenced by sampling errors.

Fig. 4. Hydrogen concentration versus depth for two Apollo 16 samples: breccia chip 68815,27 and glass spherule 68124,3. The apparently non-zero H content at negative depth (i.e., in vacuum) is due to the finite resolution (~ 200 Å) of the measurement technique. 68815,27 and 68124,3 are sealed rock box samples and were not exposed to the atmosphere.

Fig. 5. Fluorine depth profiles for Apollo 15 samples from 15427,39. The circles are plotted on half scale so that the interior fluorine in the "brown fragments" (about 60 ppm) is more easily seen.

Fig. 6. Fluorine depth profiles for a vesicle and a nearby intervesicular area of 15016,176 (Apollo 15). The vesicle profile shows a surface enhancement of fluorine while the intervesicular area does not.

Fig. 7. A schematic drawing of the energy dependence of detected protons at a lab angle of 160° for the reaction $^{12}C(d,p_o)^{13}C$. The proton energy is shown to depend on deuteron energy loss, proton energy loss, and kinematic factors. Protons emitted from the surface have the highest energy, whereas protons emitted from depth Δx have lower energies as given by the equation ($dE/dx < 0$).

Fig. 8. Upper: A proton pulse height spectrum for quartz glass showing a contamination carbon surface peak corresponding to CO or CO_2. Lower: The same sample after "sputter-cleaning" with $\sim 10^{16}/cm^2$ of 2 MeV F ions ($E_D = 1.07$ MeV).

Fig. 9.   The raw proton spectrum obtained for Apollo 11 sample 10068. The smooth curves shown are the proton spectra obtained for pure targets of ^{24}Mg, ^{27}Al and ^{28}Si that have been normalized to features characteristic of these nuclides in the spectrum for 10068. The remaining counts are from the ^{12}C in the sample. $(E_D = 1.07$ MeV.)

Fig. 10.   The points shown correspond to the background-corrected (see fig. 9) proton spectrum from carbon for Apollo 11 sample 10068,23. The two cross-hatched regions show how this spectrum has been decomposed into surface and uniform volume components, each of which has the distorted shape that is a consequence of surface roughness. The solid curve through the data is the sum of the two contributions and has $X^2 = 1.7$.

Fig. 11.   The measured surface and volume concentrations for carbon for each sample are compared. It is clear that there is no strong correlation between surface concentration and volume concentration for these samples. (Sample numbers beginning with 10 are from Apollo 11, with 15 from Apollo 15, with 6 from Apollo 16, and with 7 from Apollo 17.)
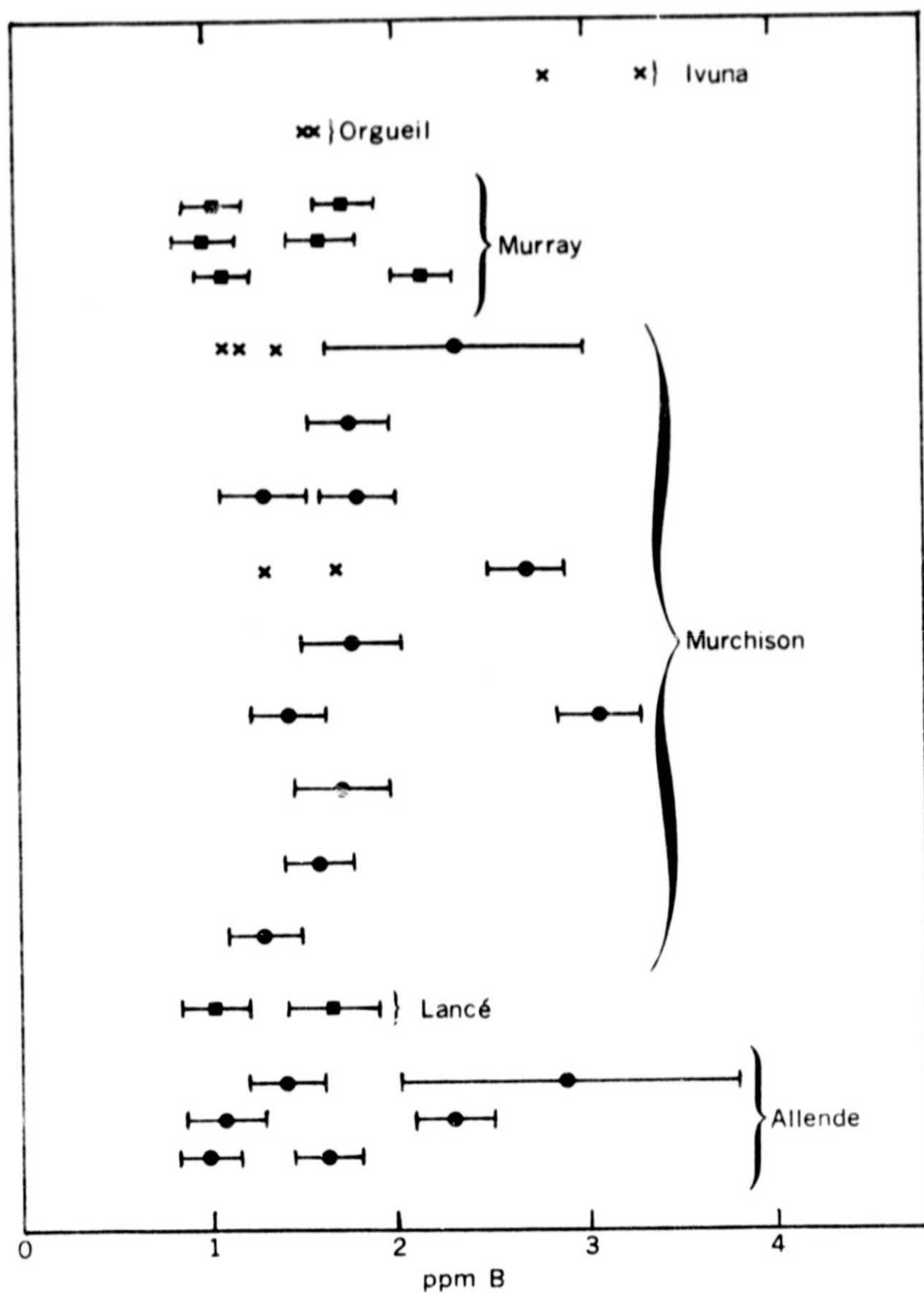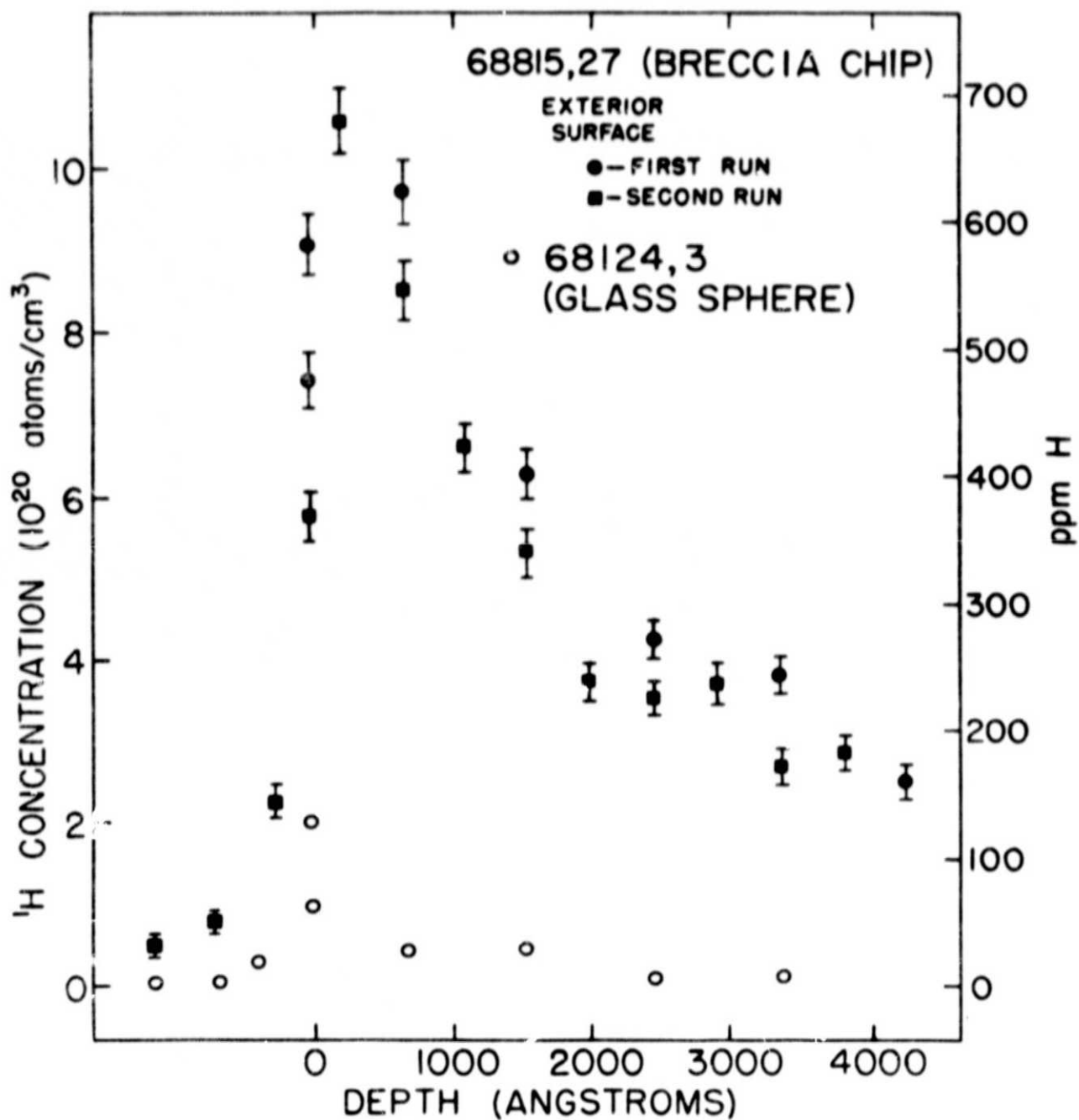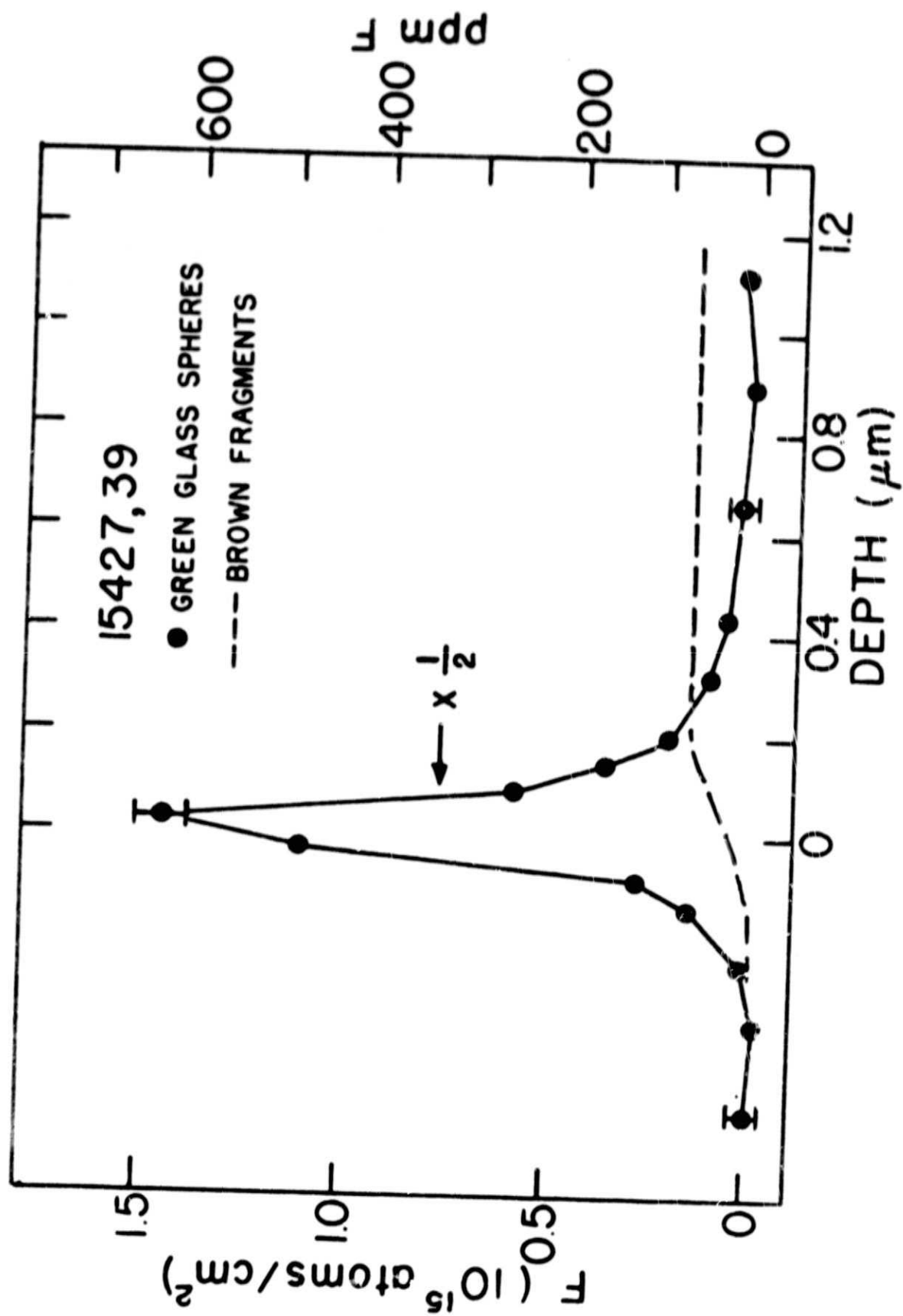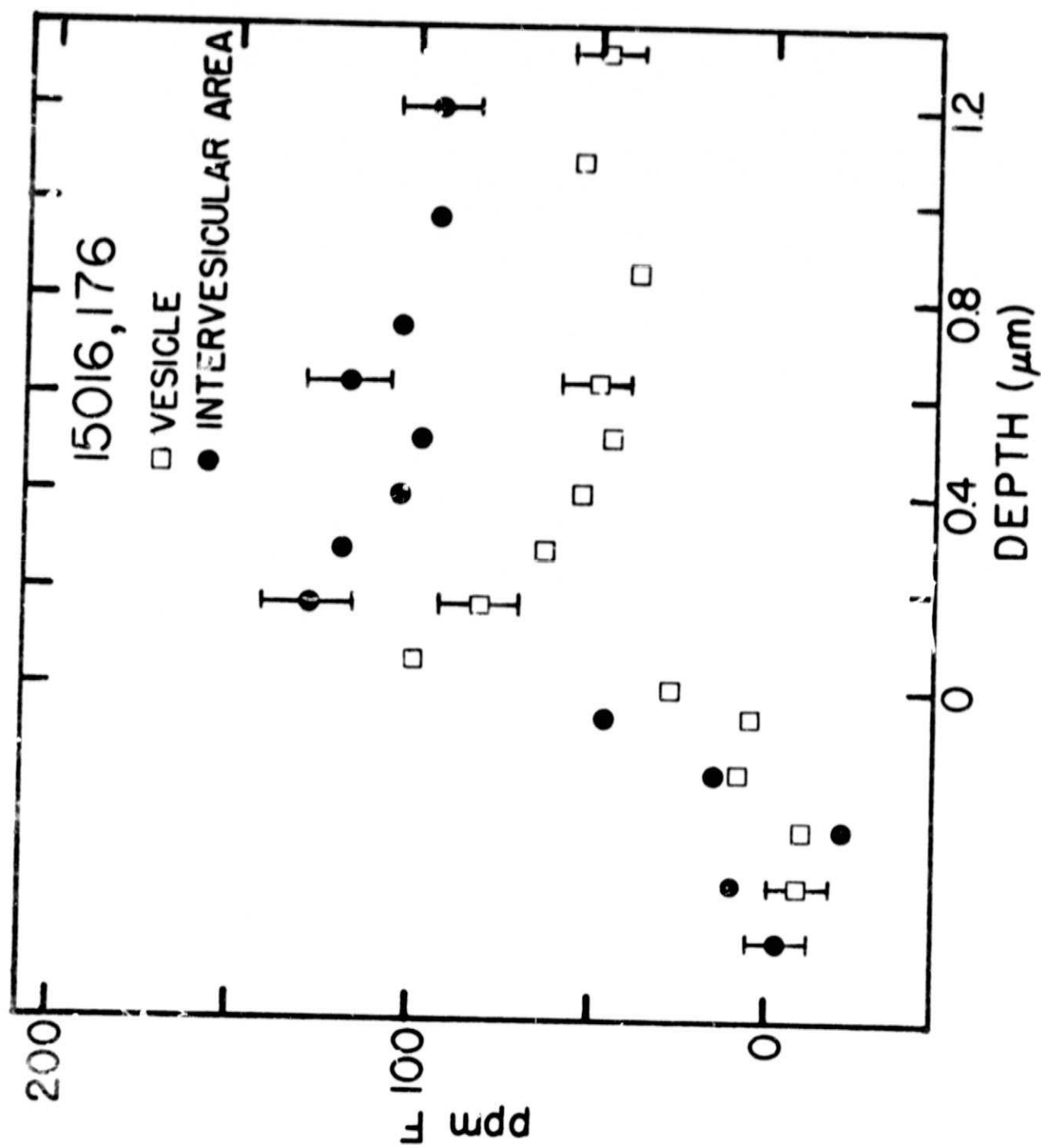
$^{11}B(d, p)^{12}B$ Counting Cycle

(a)
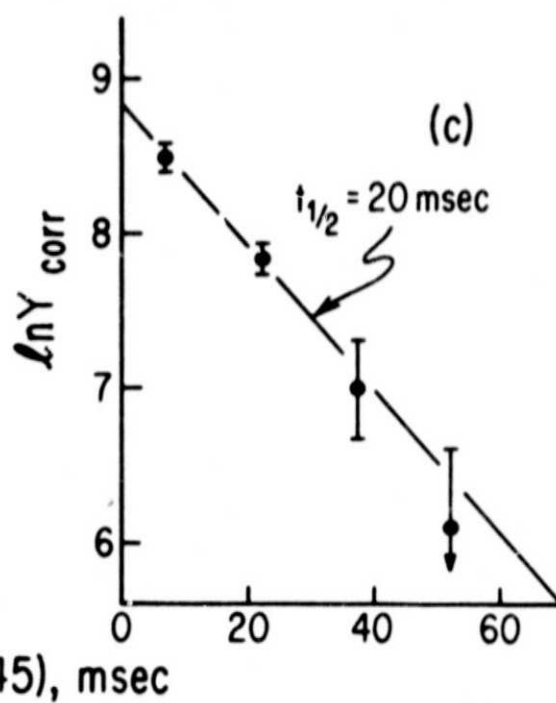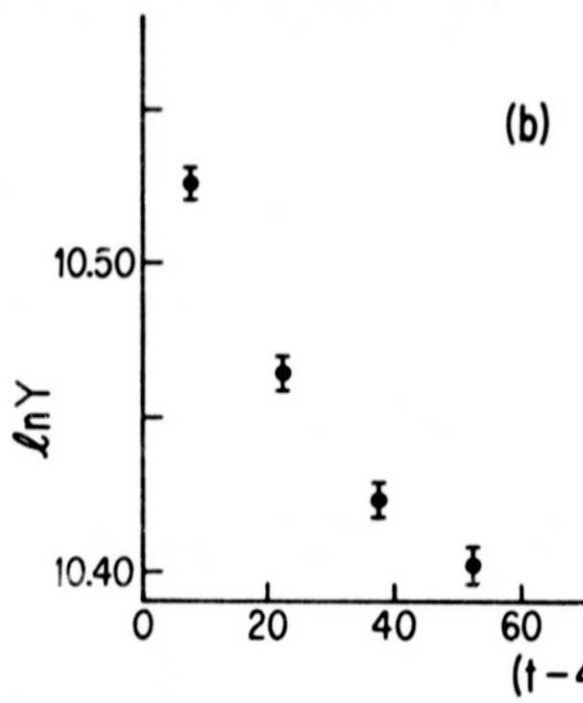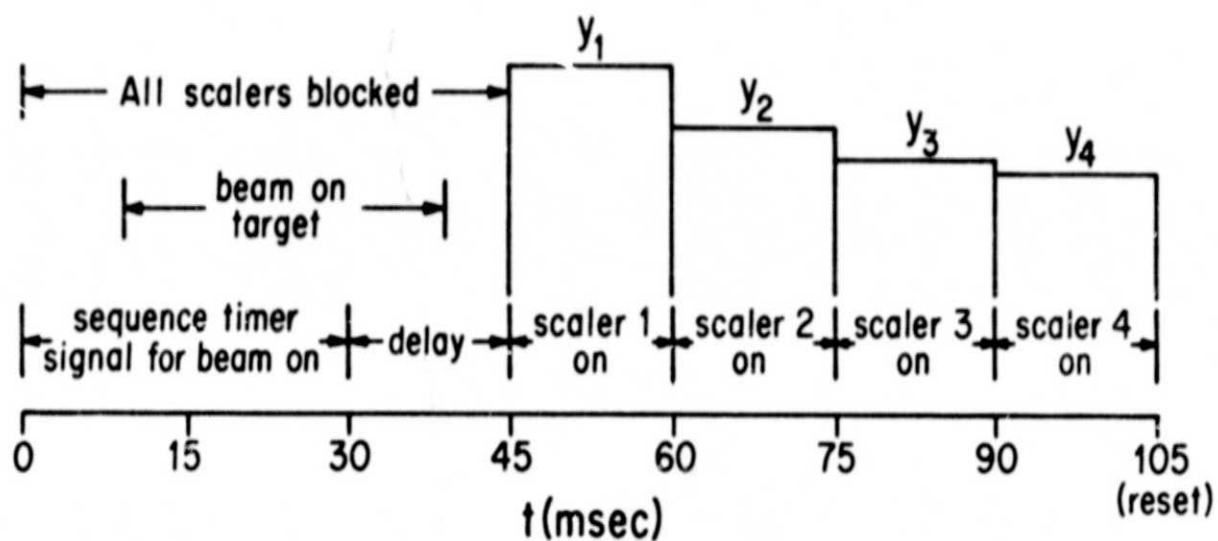
Fig. 1

Fig. 2

Fig. 3

Fig. 4

Fig. 5

Fig. 6

$$E_p = E_{p_{max}} + 0.6(E_d - E_{d_0}) + \Delta x \sec 20°(dE/dx)_p$$

$$E_d = E_{d_0} + \Delta x(dE/dx)_d$$
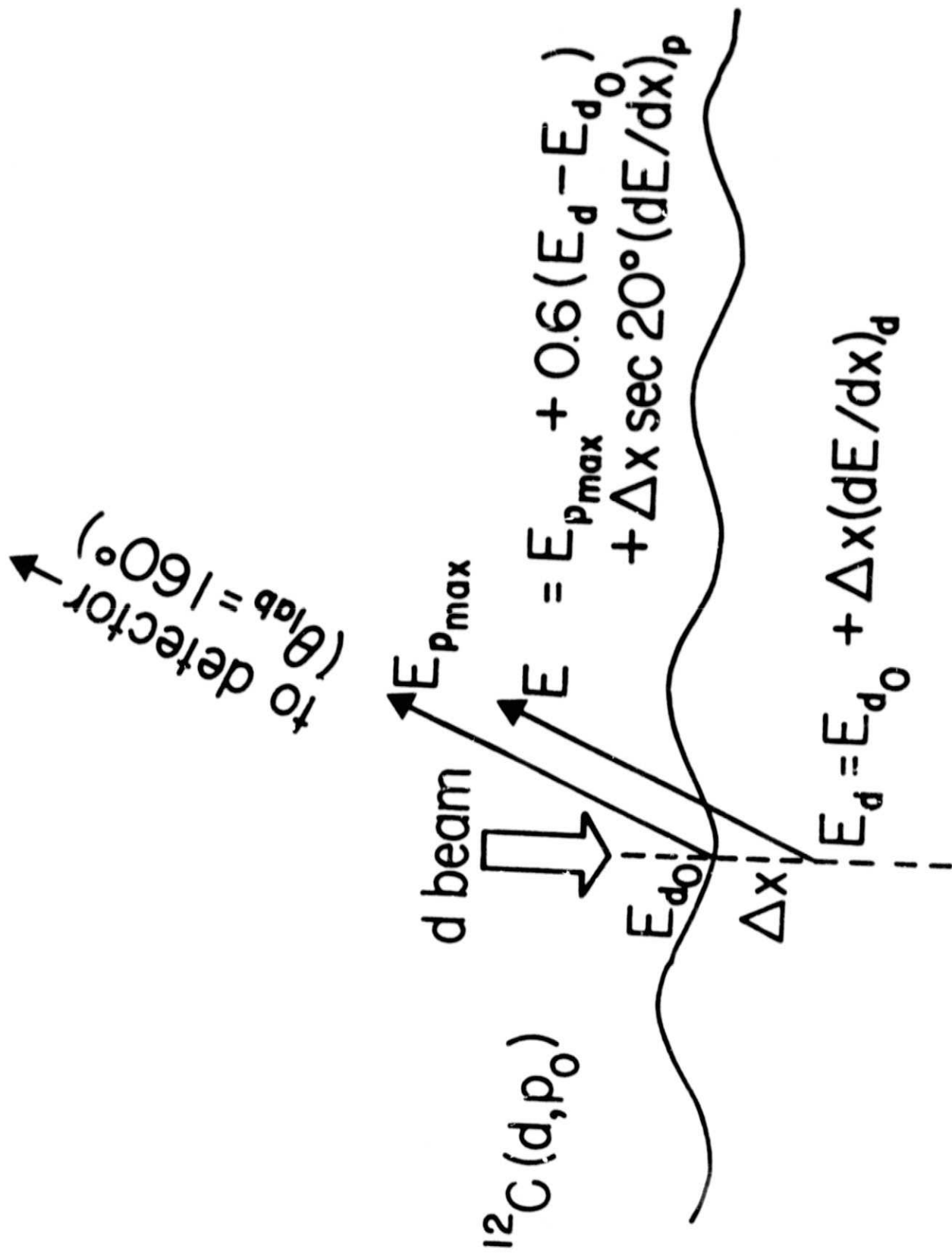
to detector
($\theta_{lab} = 160°$)
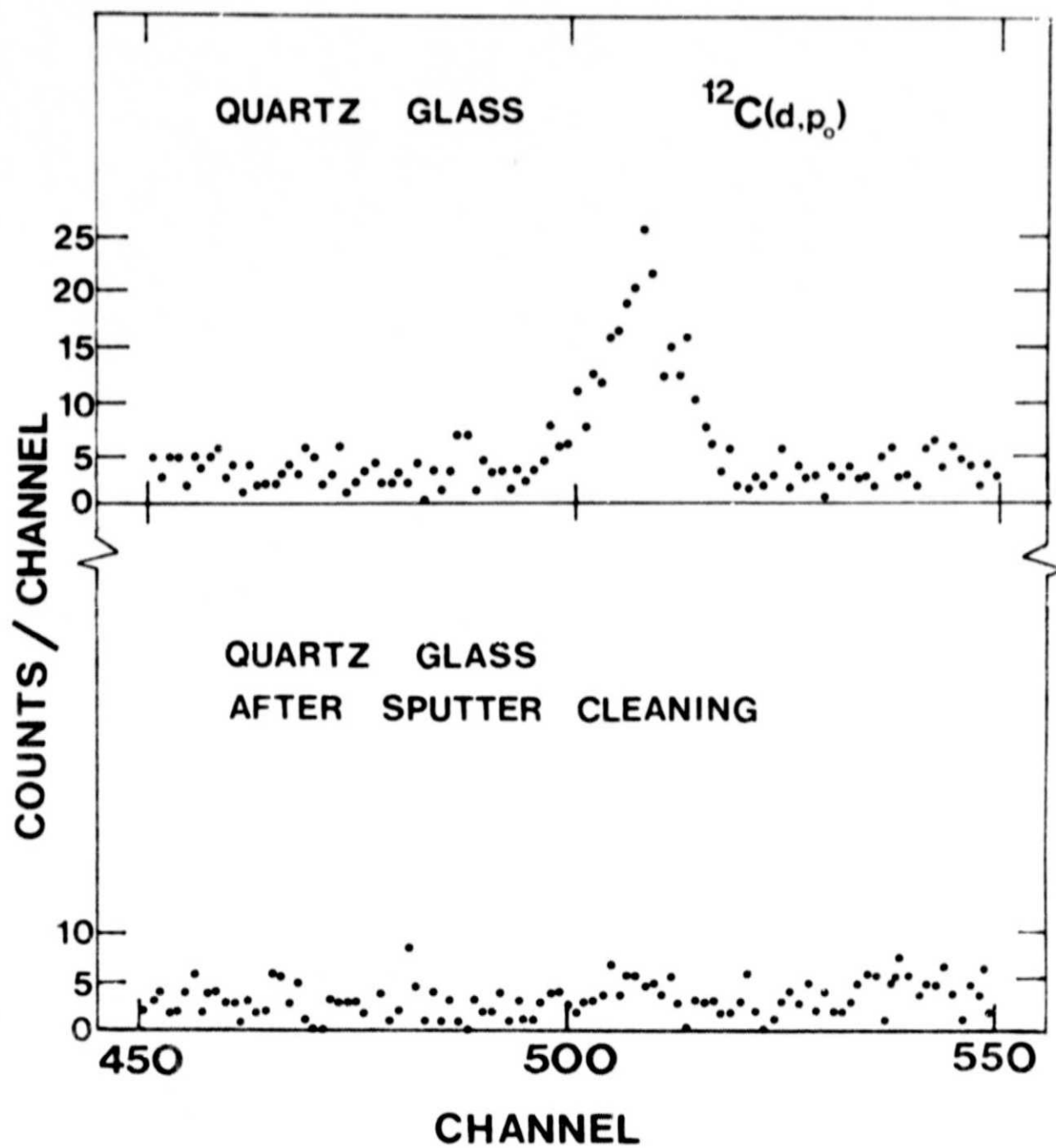
$E_{p_{max}}$

d beam

E_{d_0}

Δx

$^{12}C(d,p_0)$
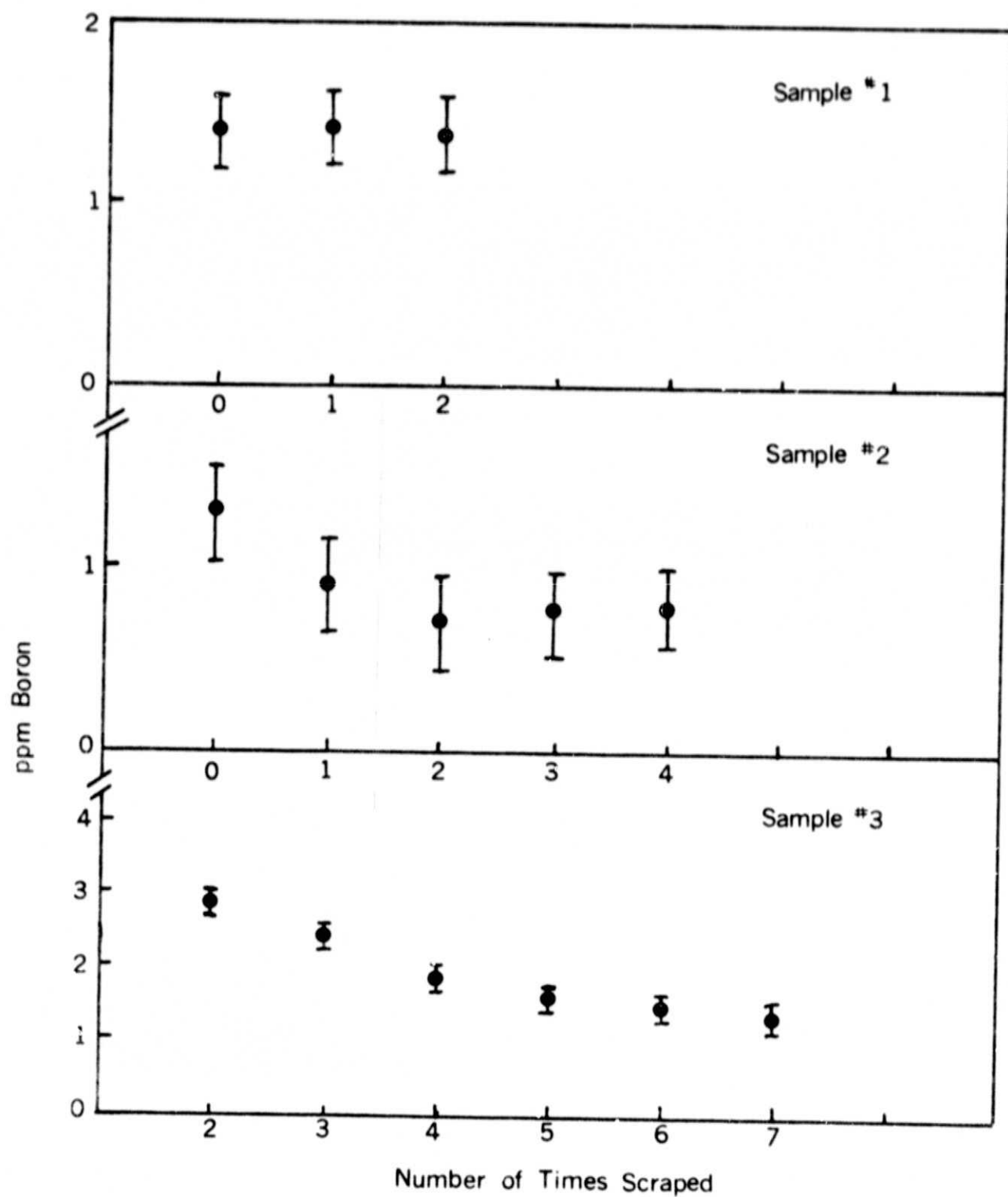
Fig. 7

Fig. 8

Fig. 9

Fig. 10

Fig. 11